

Coherent coupling of alkali atoms by random collisions

Or Katz,^{1,2} Or Peleg,² and Ofer Firstenberg^{1,*}

¹Department of Physics of Complex Systems, Weizmann Institute of Science, Rehovot 76100, Israel

²Rafael Ltd, IL-31021 Haifa, Israel

Random spin-exchange collisions in warm alkali vapor cause rapid decoherence and act to equilibrate the spin state of the atoms. In contrast, here we demonstrate experimentally and theoretically a *coherent coupling* of one alkali specie to another specie, mediated by these random collisions. We show that, the minor specie (potassium) inherits the magnetic properties of the dominant specie (rubidium), including its lifetime (T_1), coherence time (T_2), gyromagnetic ratio, and SERF magnetic-field threshold. We further show that this coupling can be completely controlled by varying the strength of the magnetic field. Finally, we explain these phenomena analytically by modes-mixing of the two species via spin-exchange collisions.

Collisions in a warm alkali vapor relax the quantum spin-state of the atoms. These collisions usually consist of a few spin-destruction collisions, limiting the lifetime (T_1), and of rapid spin-exchange collisions, limiting coherence times (T_2) [1]. Reduced coherence times affect the performance of many vapor physics applications, such as atomic clocks [2], optical memories [3, 4], and high-field magnetometers [5]. However, the spin-exchange (SE) relaxation can be completely eliminated at a regime known as spin-exchange relaxation-free (SERF) [6, 7], allowing the realization of vapor-based ultra-sensitive magnetometers [8, 9]. At other regimes, SE collisions can be utilized to incoherently transfer polarization between different atomic states [10, 11], as is widely used in the production of hyper-polarized noble gases for medical imaging [12], spin-polarized targets [13], and precision measurements [14, 15]. The incoherent transfer of polarization via SE collisions was also demonstrated in a hybrid system of two alkali species [16, 17], improving magnetometry sensitivity by optically pumping one specie at a given optical-depth and monitoring the other [18]. However, the *coherent* effects of the SE collisional interaction between different species of alkali atoms have never been investigated.

In this Letter, we demonstrate a coherent coupling of two alkali species, potassium (K) and rubidium (Rb), induced by random SE collisions. The strength of the coupling is controlled by the strength of the magnetic field. We show that at small magnetic fields, the coupling is strong and the K atoms inherit the magnetic properties of the Rb, including its gyromagnetic ratio (g) and long coherence-time (T_2). Furthermore, the lifetime (T_1) of the K atoms become that of the Rb, and the SERF magnetic-field threshold is shown to improve by an order-of-magnitude, corresponding to that of Rb. We analytically explain these phenomena by SE-induced hybridization of the quantum state of the two species.

When two alkali species co-exist in a vapor cell, each atom collides with atoms of its own specie (S) at a rate R_{SE}^{S-S} and with atoms of the other specie (S') at a rate $R_{SE}^{S-S'}$. Achieving strong coupling between the species

requires that $R_{SE}^{S-S'}$ governs the dynamics of S, exceeding both R_{SE}^{S-S} and the Larmor precession rate ω_S . The rate $R_{SE}^{S-S'} = n_{S'} \sigma_{SE}^{S-S'} \bar{v}_T$ depends on the mean thermal velocity \bar{v}_T , the alkali-alkali SE cross-section $\sigma_{SE}^{S-S'}$, and the density $n_{S'}$. For Rb and K, the mutual cross-section $\sigma_{SE}^{Rb-K} \approx 2 \cdot 10^{-14} \text{ cm}^{-2}$ is similar to the self cross-sections $\sigma_{SE}^{K-K} = 1.5 \cdot 10^{-14} \text{ cm}^{-2}$ and $\sigma_{SE}^{Rb-Rb} = 1.9 \cdot 10^{-14} \text{ cm}^{-2}$ [19]. When the two alkali drops are not mixed, the Rb vapor density n_{Rb} is 10 times higher than the K density n_K [20]. That is, the SE rate experienced by the K is predominantly determined by the collisions with Rb, $R_{SE}^{K-Rb} \sim 10 R_{SE}^{K-K}$, whereas the Rb is only weakly affected by the presence of the K since $R_{SE}^{Rb-Rb} \sim 10 R_{SE}^{Rb-K}$. Thus, at high SE rates the K dynamics will be significantly affected by the presence of the Rb.

To probe the magnetic coherence of the two species we use a single pump and two probe beams as shown in Fig. 1. We use a spherical cell of radius 0.5" with natural abundance of Rb (72% ^{85}Rb and 28% ^{87}Rb) and K, in two separate drops. The cell is heated to a temperature of $T = 95^\circ\text{C}$, corresponding to number densities of

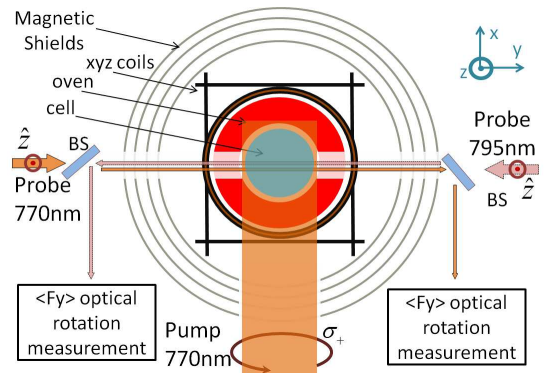


Figure 1. Schematics of the experimental setup. The K atoms are initially polarized by a σ_+ -polarized pumping beam. The polarization rotation of two linearly-polarized beams (770 nm and 795 nm) is measured to probe the atomic spin precession of both K and Rb atoms, after a magnetic field B_z is applied. BS: non-polarizing beam splitter.

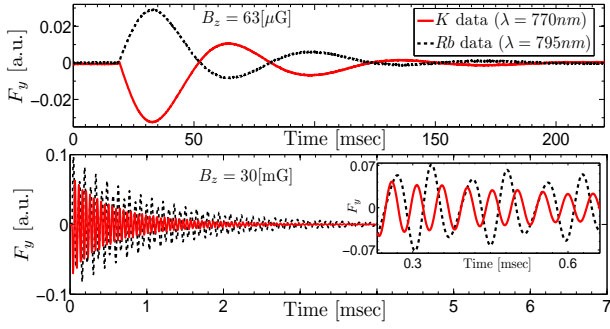


Figure 2. Typical measurement of F_y (the \hat{y} component of the spin) for K and Rb. At low magnetic fields (top), the two species are coherently coupled- oscillate and decay at the same rate, while at high magnetic fields (bottom), they are decoupled- oscillate and decay differently.

$n_{\text{Rb}} \sim 4 \cdot 10^{12} \text{ cm}^{-3}$ and $n_{\text{K}} \sim 4 \cdot 10^{11} \text{ cm}^{-3}$. We reduce radiation trapping and collision rate with the cell walls by introducing 200 torr of N_2 buffer gas. The magnetic field is controlled by shielding the cell with μ -metal cylinders and three perpendicular Helmholtz coils. We optically pump the K using a circularly-polarized laser beam at 770 nm along the \hat{x} direction. The beam is wider than the cell with intensity of 1 mW/cm^2 , tuned to the $D1$ absorption peak. During the pumping, the K atoms pump the Rb atoms via SE collisions. We then switch off the pumping light and apply a magnetic field $B\hat{z}$. Consequently, both Rb and K spins precess around the magnetic field while decaying due to the various relaxation mechanisms in the cell. We monitor this precession by measuring the optical rotation of linearly-polarized probe beams at 770 nm and 795 nm, close to resonance with the K and Rb, respectively. We ensure that the probes do not induce relaxation by using moderate intensities ($I_{\text{Rb}} = 1 \text{ mW/cm}^2$, $I_{\text{K}} = 10 \text{ mW/cm}^2$) and detuning from the $D1$ line [$\Delta\nu_{\text{Rb}} = 25 (2\pi)\text{GHz}$, $\Delta\nu_{\text{K}} = 15 (2\pi)\text{GHz}$]. As a reference, we measured the magnetic coherence of K in a similar cell, without Rb.

A typical measurement of the optical rotation signals at low and high magnetic fields is shown in Fig. 2. At high magnetic fields, the two species are weakly coupled and oscillate at different frequencies $\omega_{\text{K}} = 1.5 \cdot \omega_{\text{Rb}}$, corresponding to their natural gyromagnetic ratios [6],

$$g = \frac{\mu_B g_s}{\hbar} \frac{1}{(2I + 1)}, \quad (1)$$

where $I_{s_{\text{Rb}}} = 5/2$, $I_{\text{K}} = 3/2$, and $g_s = 2$. However at low magnetic fields, the two species are strongly coupled and thus precess at the same frequency and have the same decoherence rate. The frequencies and decoherence rates were determined by fitting each signal to the simple model $f = \sum_{i=1,2} c_i e^{-\Gamma_i t} \sin(\omega_i t + \varphi_i)$ assuming that $c_i, \Gamma_i, \omega_i,$ and φ_i are constants. We note that the 180° phase between the signals results from the counter-propagating arrangement of the probing beams. The

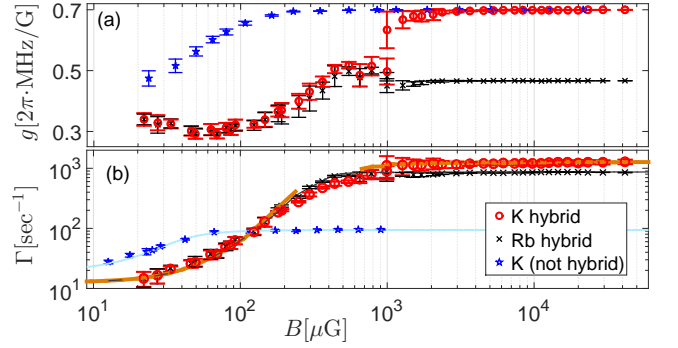


Figure 3. (a). Measured gyromagnetic ratios $g = \omega/B_z$ of Rb (black) and K (red) in the hybrid cell. The K inherits the precession rate of Rb at low magnetic fields. The measured g of K in a reference cell without Rb is shown for comparison (blue). (b) Measured decoherence rate $\Gamma = 1/T_2$ of the two species. Γ_{K} is significantly improved at low magnetic fields. Both species experience SERF at the same magnetic-field threshold, 10 times higher than the threshold of K without Rb. The solid lines are the analytically-calculated values.

beating of the Rb signal (Fig. 2 bottom) originated from the presence of the ^{87}Rb isotope, and its effect on the K dynamics is discussed in the supplemental material [21]. At low and at high magnetic fields, each signal has a single dominant precession rate ω_i with a corresponding decoherence rate Γ_i . Therefore in these regimes, we identify for each specie the dominant precession rate ω_{K} , ω_{Rb} and decoherence rate Γ_{K} , Γ_{Rb} , shown in Fig. 3.

The *coherent* coupling is demonstrated in Fig. 3a by examining the precession rates of the two species. While the gyromagnetic ratio of the Rb is practically unaffected by the presence of the K (corresponding to its normal SERF behavior [6, 7]), the K dynamics is strongly influenced by the Rb. At high magnetic fields, the K is well decoupled and precesses at its natural rate, $g = 0.7 (2\pi)\text{MHz/G}$. However, at low magnetic fields, the coupling is strong and the K precesses at the gyromagnetic ratio of Rb, $g = 0.26 (2\pi)\text{MHz/G}$, and not at its natural low-field precession rate [6, 7], $g = 0.46 (2\pi)\text{MHz/G}$.

To investigate the transition between the coupled and uncoupled states of the two species, we show in Fig. 4 the spectral dependence of the signals on the applied magnetic field. We plot the FFT of the measured signals at different magnetic fields using a normalized scale ($\omega \rightarrow \omega/B_z$) corresponding to the gyromagnetic ratio g (for visualization purposes, we replace with zero the FFT around $g = 0$). At high and low magnetic fields, the physics is exactly the same as in Fig. 3a: the two species share the same gyromagnetic ratio (that of the Rb) at low fields, while reaching their normal different values at high magnetic fields. However at intermediate fields, the K precesses at a combination of two frequencies, both at its natural precession rate and at the rate of ^{85}Rb

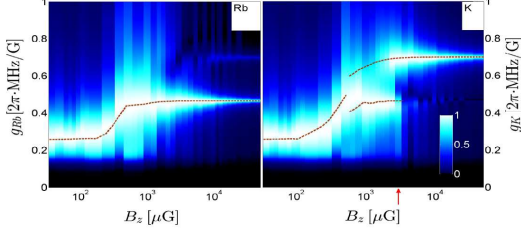


Figure 4. Spectral content of the measured signals as a function of the magnetic field. The vertical axis is scaled to measure the gyromagnetic ratio. The Rb precesses at a single rate (left) while the K inherits the rate of the Rb at low fields. The theoretical g is plotted in dashed lines.

(most clearly visible at $B_z=3$ mG, red arrow in Fig. 4). The nature of this transition can not be explained by a mere shift in the slowing-down-factor since the K dynamics consists of two distinct frequencies. Thus, the minor specie (K) is coherently coupled to the dominant specie (Rb) at low magnetic fields by SE collisions, and the coupling strength is controlled by the magnitude of the magnetic field.

This coherent coupling alters significantly other important properties of the K. While the relaxation rate $\Gamma_{Rb}(B_z)$ is unaffected by collisions with K (SE relaxation is eliminated at $\omega_{Rb} \lesssim R_{SE}^{Rb-Rb}$ [6], as if the K is absent), the relaxation rate $\Gamma_K(B_z)$ is inherited from the Rb, as shown in Fig. 3b. Consequently, the relaxation rate $\Gamma_K(B_z)$ decreases dramatically at low magnetic fields, in comparison to a cell without Rb. The elimination of relaxation of the K atoms appears at $\omega_K \lesssim R_{SE}^{Rb-K}$, *i.e.* at magnetic fields 10-times higher (less stringent) than those required without the Rb, $\omega_K \lesssim R_{SE}^{K-K}$. Thus, the dominant specie (Rb) drives the minor specie (K) into SERF at the magnetic-field threshold of the dominant specie. At high magnetic fields, the relaxation of the minor specie is increased due to mutual SE collisions. Furthermore, we measure an identical lifetime of both species ($T_1 = 86 \pm 1$ msec). Via collisions, the K inherits the lifetime of the Rb incoherently, as theoretically explained for different isotopes in [11]. Since the spin destruction is dominated by electron-randomizing collisions (*e.g.*, anisotropic collisions with N_2), the K benefits from the larger nuclear spin reservoir of the Rb. Therefore, through collisional induced coherent coupling, the minor specie (K) inherits the magnetic properties of the dominant specie (Rb), including its precession rate, decoherence rate, lifetime, and SERF magnetic field threshold.

To understand the nature of the coherent coupling, we solve the coupled Liouville equations describing the dynamics of the system. Due to frequent SE collisions, the coherence between the two hyperfine levels decays rapidly. Therefore, the ground-state density ma-

trix of each specie s can be simplified by decomposing ρ^s into a two block diagonal form $\rho^s = \rho_a^s + \rho_b^s$, where $a = I_s + 1/2$ denotes the higher hyperfine level and $b = I_s - 1/2$ the lower one [22]. The Larmor coherence can be described by the transverse spin vector $\langle F_+^s \rangle \equiv -F_x^s + iF_y^s = F_{a+}^s + F_{b+}^s$, where we omit the brackets $\langle \rangle$ for brevity. In the absence of the mutual SE interaction, the dynamics of F_+^s for each specie is given by [21]

$$\frac{d}{dt} \begin{pmatrix} F_{a+}^s \\ F_{b+}^s \end{pmatrix} = \begin{pmatrix} -ig_s B_z & 1 & 0 \\ 0 & -1 \end{pmatrix} - R_{SE}^{s-s} \begin{pmatrix} x_a^s & y^s \\ y^s & x_b^s \end{pmatrix} - R_{SD}^{s-s} \begin{pmatrix} w_a^s & z^s \\ z^s & w_b^s \end{pmatrix} \begin{pmatrix} F_{a+}^s \\ F_{b+}^s \end{pmatrix}, \quad (2)$$

where g_s is the gyromagnetic ratio of each specie [Eq. (1)], R_{SD}^{s-s} is the spin-destruction rate, and the constant coefficients $w_a^s, w_b^s, x_a^s, x_b^s, y^s, z^s$ are given in [21], depending on the nuclear spin I_s only. The SE coupling between the two species supplements Eq. (2) by inducing the coupling interaction

$$\frac{d}{dt} \left(\tilde{\mathbf{F}}_+ \right)_{coupling} = -\overleftrightarrow{\mathbf{M}} \cdot \tilde{\mathbf{F}}_+, \quad (3)$$

where $\tilde{\mathbf{F}}_+$ denotes the 4-component vector $\tilde{\mathbf{F}}_+ \equiv (F_{a+}^{Rb}, F_{b+}^{Rb}, F_{a+}^K, F_{b+}^K)$ and $\overleftrightarrow{\mathbf{M}}$ is the 4×4 linearized SE coupling matrix, given by

$$\overleftrightarrow{\mathbf{M}} = diag \begin{pmatrix} R_{SE}^{Rb-K} \\ R_{SE}^{Rb-K} \\ R_{SE}^{K-Rb} \\ R_{SE}^{K-Rb} \end{pmatrix} \cdot \begin{pmatrix} w_a^{Rb} & z^{Rb} & G_{11}^{Rb} & G_{12}^{Rb} \\ z^{Rb} & w_b^{Rb} & G_{21}^{Rb} & G_{22}^{Rb} \\ G_{11}^K & G_{21}^K & w_a^K & z^K \\ G_{12}^K & G_{22}^K & z^K & w_b^K \end{pmatrix}. \quad (4)$$

Here, the constants $G_{11}^s, G_{12}^s, G_{21}^s, G_{22}^s$ depend on I_{Rb} and I_K only [21]. Qualitatively, this coupling interaction has two major effects on the dynamics of the vapor. First, it increases the effective spin-destruction rate of the two species, by R_{SE}^{Rb-K} for the Rb and R_{SE}^{K-Rb} for the K, as can be seen by the block-diagonal elements in Eq. (4). Second, since $R_{SE}^{K-Rb} \gg R_{SE}^{K-K}, R_{SD}^{K-K}$, the coupling through the coefficients G_{ij}^K becomes the dominant collisional interaction for the K, while the coupling experienced by the Rb is weak, since $R_{SE}^{Rb-K} \ll R_{SE}^{Rb-Rb}$. At low magnetic fields, R_{SE}^{K-Rb} is the dominant rate for the K spins, which therefore respond to the precession of the Rb spins as forced oscillations and inherit the Rb magnetic properties. At the same time, the Rb dynamics remain unaffected by the K.

To quantitatively describe this coupling, we solve the two coupled Eqs. (2)-(3) by diagonalizing the 4×4 matrix and calculating the eigenvalues λ_i of the four eigenmodes $|\lambda_i\rangle$. Each spin component of $\tilde{\mathbf{F}}_+^i$ can be spanned by the eigenmodes,

$$\tilde{\mathbf{F}}_+^i(t) = \tilde{\mathbf{F}}_+^i(0) \sum_{j=1}^4 p_{ij} e^{\lambda_j t}, \quad (5)$$

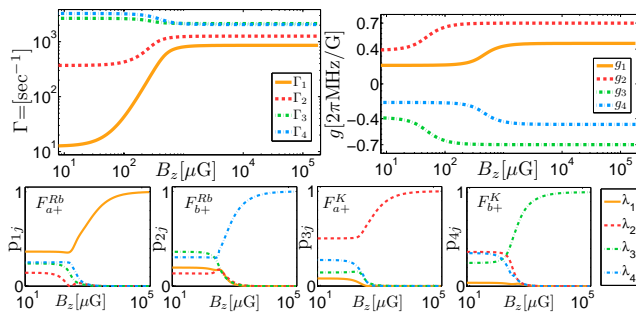


Figure 5. Theoretical results. Top: Decoherence rates $-\text{Re}(\lambda)$ (left) and gyromagnetic ratios $\text{Im}(\lambda/B_z)$ (right) of the four eigenmodes. The decoherence rate Γ_1 vanishes at low magnetic fields due to SERF. Bottom: The coupling coefficients p_{ij} of the four spin components. At high magnetic fields, the spins of K and ^{85}Rb consist of a single mode; at low fields, the spins consist of all modes, and thus share their coherence.

where the coefficients p_{ij} satisfy the normalization condition $\sum_j p_{ij} = 1$. The decoherence rates and gyromagnetic ratios of the eigenmodes, corresponding to $\Gamma_i = -\text{Re}(\lambda_i)$ and $g_i = \text{Im}(\lambda_i/B_z)$ respectively, are shown in Fig. 5 (top). At high magnetic fields, the gyromagnetic ratios $g_1 = -g_4 = 0.47(2\pi)\text{MHz/G}$ correspond to the precession rate of ^{85}Rb , while $g_2 = -g_3 = 0.7(2\pi)\text{MHz/G}$ correspond to the rate of K [Eq. (1)]. The sign of g corresponds to the co-rotation of the upper hyperfine level (a) for a positive value and counter-rotation of the lower level (b) for a negative value. Γ_1 remains the lowest decay rate of the system at all magnetic fields. As the magnetic field is lowered, $\Gamma_1(B)$ decreases (experiencing SERF), and consequently $|\lambda_1\rangle$ becomes the dominant eigenmode.

To infer the dynamics of the atoms, we plot the coefficients p_{ij} of each specie in Fig. 5 (bottom). At high magnetic fields, the eigenmodes are well resolved, corresponding to $|\lambda_1\rangle$ for F_{a+}^{Rb} , $|\lambda_2\rangle$ for F_{a+}^{K} , $|\lambda_3\rangle$ for F_{b+}^{Rb} , and $|\lambda_4\rangle$ for F_{b+}^{K} . Consequently, the different hyperfine levels remain resolved, such that each magnetic coherence rotates at its natural rate g_i . As the magnetic field is lowered, $\tilde{\mathbf{F}}_+^i$ becomes a mixture of the four different modes, inducing mixing between the different hyperfine levels of both species. Since at low magnetic fields $\Gamma_1 \ll \Gamma_2, \Gamma_3, \Gamma_4$, eigenmode $|\lambda_1\rangle$ dominates; The K and Rb spins precess and decay at the same rate and experience SERF at the Rb's transition rate. This common effectively-single eigenmode shows that, at low magnetic fields, the two species hybridize by the SE interaction. At intermediate magnetic fields, Γ_1 increases and more eigenmodes become important, resulting in multiple decoherence and precession rates for each specie, especially for the minor one (K). At this transition regime, the high decoherence rates $\Gamma_i \gtrsim \omega_i - \omega_j$ broaden the spectral profile of the signals, as observed in Fig. 4.

To compare with the experiment, the theoretical decoherence rate and gyromagnetic ratio are plotted in Figs. 3 and 4. These parameters were evaluated from Eq. (5), while taking into account the presence of ^{87}Rb in our experiment [21], without any free parameters. Γ_{Rb} is almost unaffected by the presence of K and has a single decoherence rate and gyromagnetic ratio at any magnetic field. The K is governed by a single mode at low and high magnetic fields and by multiple modes at intermediate fields. Therefore at this region, we do not associate a single Γ_{K} and show the two dominant frequencies in Fig. 4. Our theoretical model, appears to fully describe the physics of the interaction and the hybridization of the species.

The SE-hybridization of different alkali species might be utilized in magnetometry and quantum-information applications. In magnetometry, one can benefit from the SERF properties of the dominant specie while monitoring the state of the minor specie, especially when applied in hybrid magnetometers schemes [18] using a single laser. For quantum-information applications, the hybridization could introduce a new mechanism to interface vapor-based quantum memories.

In conclusion, we have shown that random SE collisions coherently couple two different alkali species. The coupling strength is controlled by the magnitude of the magnetic field. At low magnetic fields, a minor specie is strongly coupled to the dominant specie and as a result inherits the magnetic properties of the dominant specie, such as the coherence-time and gyromagnetic ratio. At intermediate magnetic fields, we measure a unique response of the minor specie, consisting of two precession rates. At high magnetic fields, the two species become decoupled. We explain these phenomena by showing analytically that, by lowering the magnetic field, the minor specie starts sharing the main eigenmode of the dominant specie. This effect may be utilized in different magnetometry and quantum-information schemes.

We thank Mark Dikopoltsev and Elad Greenfeld for their valuable help in preparing the cell. This work was supported by the Israel Science Foundation and the Zumbi Stiftung.

* Corresponding author:ofer.firstenberg@weizmann.ac.il

- [1] W. Happer, Rev. Mod. Phys. 44, 169 (1972).
- [2] S. A. Zibrov, I. Novikova, D. F. Phillips, R. L. Walsworth, A. S. Zibrov, V. L. Velichansky, A. V. Taichenachev, and V. I. Yudin, Phys. Rev. A 81, 013833 (2010).
- [3] D. F. Phillips, A. Fleischhauer, A. Mair, R. L. Walsworth, and M. D. Lukin, Phys. Rev. Lett. 86, 783 (2001).
- [4] M. Shuker, O. Firstenberg, R. Pugatch, A. Ron, and N. Davidson, Phys. Rev. Lett. 100, 223601 (2008).
- [5] D. Budker and M. V. Romalis, Nat. Phys. 3, 227 (2007).
- [6] W. Happer and A. C. Tam, Phys. Rev. A 16, 1877 (1977).
- [7] O. Katz, M. Dikopoltsev, O. Peleg, M. Shuker, J. Stein-

- hauer, and N. Katz, Phys. Rev. Lett. 110, 263004 (2013).
- [8] J. C. Allred, R. N. Lyman, T. W. Kornack, and M. V. Romalis, Phys. Rev. Lett. 89, 130801 (2002).
- [9] R. Mhaskar, S. Knappe, and J. Kitching, Appl. Phys. Lett. 101, 241105 (2012).
- [10] T. G. Walker and W. Happer, Rev. Mod. Phys. 69, 629 (1997).
- [11] S. Appelt, A. B. Baranga, C. J. Erickson, M. Romalis, A. R. Young, and W. Happer, Phys. Rev. A 58, 1412 (1998).
- [12] S. B. Fain, F. R. Korosec, J. H. Holmes, R. O'Halloran, R. L. Sorkness, and T. M. Grist, Magn. Reson. Imaging, 25, 910-23 (2007).
- [13] T. Katabuchi, S. Buscemi, J. M. Cesaratto, T. B. Clegg, T. V. Daniels, M. Fassler, R. B. Neufeld and S. Kadlecek, Rev. Sci. Instrum. 76, 033503 (2005).
- [14] G. Vasilakis, J. M. Brown, T. W. Kornack, and M. V. Romalis, Phys. Rev. Lett. 103, 261801 (2009).
- [15] M. Smiciklas, J. M. Brown, L. W. Cheuk, S. J. Smullin, and M. V. Romalis, Phys. Rev. Lett. 107, 171604 (2011).
- [16] E. Babcock, I. Nelson, S. Kadlecek, B. Driehuys, L. W. Anderson, F. W. Hersman and T. G. Walker, Phys. Rev. Lett. 91, 123003 (2003).
- [17] B. Lanco and T. G. Walker, Phys. Rev. A 83, 065401 (2011).
- [18] M. V. Romalis, Phys. Rev. Lett. 105, 243001 (2010).
- [19] since the collisions involve only the outer electrons of the colliding pair [1].
- [20] D. Lide., Handbook of Chemistry and Physics (CRC, 2004), 85th ed.
- [21] See Supplemental Material at ["URL will be inserted by publisher"] for a comprehensive description of Bloch equations derivation and the effect of ^{87}Rb on the dynamics of the vapor.
- [22] I. M. Savukov and M. V. Romalis, Phys. Rev. A 71, 023405 (2005).